Theor Chem Acc (2011) 130:1145–1154
DOI 10.1007/s00214-011-1049-y

REGULAR ARTICLE

Systematic mutational analysis of an ubiquitin ligase (MDM2)-binding peptide: computational studies

Yun Liu · David P. Lane · Chandra S. Verma

Received: 21 July 2011 / Accepted: 16 September 2011 / Published online: 5 October 2011

Abstract To understand the importance of amino acids that comprise the peptide PMI (p53-MDM2/MDMX inhibitor), a p53-mimicking peptide with high affinity for the ubiquitin ligase MDM2, computational alanine scanning has been carried out using various protocols. This approach is very useful for identifying regions of a peptide that can be mutated to yield peptides that bind to their targets with higher affinities. Computational alanine scanning is a very useful technique that involves mutating each amino acid of the peptide in its complex with its target (MDM2 in the current study) to alanine, running short simulations on the mutated complex and computing the difference in interaction energies between the mutant peptides and the target protein (MDM2 in the current study) relative to the interaction energy of the original (wild-type) peptide and the target protein (MDM2 in the current study). We find that running multiple short simulations yield values of computed binding affinities (enthalpies) that are similar to those obtained from a long simulation and are well correlated with the trends in the data available from experiments that used Surface Plasmon Resonance to obtain dissociation constants. The p53-mimicking peptides contain three amino acids (F19, W23 and L26) that are major determinants of the interactions between the peptides and MDM2 and form an essential motif. We find in the current study that the trends amongst the contributions to experimental binding affinities of the hydrophobic residues F19, W23 and L26 are the best reproduced in all the computational protocols examined here. This study suggests that running such short simulations may provide a rapid method to redesign peptides to obtain high-affinity variants against a target protein. We further observe that modelling an extended conformation at the C-terminus of the helical PMI peptides, in accord with the conformation of the p53-peptide complexed to MDM2, reproduces the trends seen amongst the experimental affinities of the peptides that carry the alanine mutations at their C-termini. This suggests that some of the mutant peptides possibly interconvert between helical and extended states and can bind to MDM2 in either conformation. This novel feature, not obvious from the crystallographic data, if factored into modelling protocols, may yield novel high-affinity peptides. Our findings suggest that such protocols may enable rapid investigations of at least certain types of amino acid mutations, notably from large to small amino acids.

Keywords p53 · MDM2 · Peptide · Mutagenesis · Simulations

Dedicated to Professor Akira Imamura on the occasion of his 77th birthday and published as part of the Imamura Festschrift Issue.

Y. Liu · C. S. Verma (✉)
Bioinformatics Institute (A*STAR), 30 Biopolis Street, 07-01 Matrix, Singapore 138671, Singapore
e-mail: chandra@bii.a-star.edu.sg

D. P. Lane
p53 Laboratory (A*STAR), 8A Biomedical Grove 06-06, Singapore 138648, Singapore

C. S. Verma
Department of Biological Sciences, National University of Singapore, 14 Science Drive 4, Singapore 117543, Singapore

C. S. Verma
School of Biological Sciences, Nanyang Technological University, 60 Nanyang Drive, Singapore 637551, Singapore

1 Introduction

The P53 protein is a tumour suppressor that protects cells from various types of stresses by transcribing genes that

modulate cell cycle, apoptosis and senescence [1]. Its surveillance (for example checking for errors such as DNA damage) and maintenance of genomic integrity are under the control of several ligases of which the ubiquitin ligase MDM2 (Murine Double Minute) is the most researched [2]. MDM2 and p53 are engaged in a negative feedback loop whereby MDM2 degrades p53 and p53 transcribes MDM2. Under normal conditions, MDM2 sequesters p53 for degradation; upon stress, various post-translational modifications release p53 from MDM2 [3]. MDM2 interacts with p53 through at least two sites—the N-terminal domains of both bind to each other, while there is an interaction between MDM2 and the DNA-binding domain of p53 [4]. The interaction between the N-terminal transactivation domain of p53 with MDM2 [5] hinges on three critical residues in p53—F19, W23 and L26, which are conserved [6]; structural, mutational and computational studies have revealed that these three residues (F19, W23, L26 highlighted in Fig. 1a) contribute the maximal binding energy to the interaction (Fig. 1a). The three residues are located on the hydrophobic face of an amphipathic helix adopted by this segment of p53. This results in their spatial disposition such that they embed in the largely hydrophobic-binding pocket of MDM2. The structure of the three residues is also important to ensure a good fit in their respective binding "pockets" in MDM2, although L26 is most tolerant to certain substitutions. Interruption of the N-terminal domain interactions between p53 and MDM2 has been shown in various in vitro and in vivo models to activate p53 and causes cancer cells to die either through apoptosis or senescence [7]. p53 has been directly or indirectly implicated in most human cancers either through a mutation in the gene or in some component of the pathway. In a subset of cancers, while p53 itself is unmodified, MDM2 is highly over-expressed [8, 9]. These cancers become promising targets for small molecules and peptides that bind MDM2 and disrupt the interaction between the N-termini of both MDM2 and p53. Indeed several small molecules and peptides have been developed/designed for this purpose and some are already in clinical trials [10]. In one such effort, phage display yielded one of the most potent peptides called PMI [11] with sequence TS**F**AEY**W**NL**L**SP (the amino acids in bold correspond to the 3 conserved amino acids F19, W23 and L26, Fig. 1b); this peptide bound to MDM2 at least two orders of magnitude stronger than a peptide of the same length with the wild-type p53 sequence (ET**F**SDL**W**KL**L**PE). While the three residues, F, W and L (in bold) contribute a significant amount of binding energy, neighbouring residues also contribute small amounts that can yield a non-trivial total contribution [12] and this has become abundantly clear from the work on the PMI mutants [13]. In order to examine the role of all residues in this peptide, the authors subsequently carried out an alanine scan of the entire peptide and found that while the majority of the binding energy arises from these three hydrophobic residues and additionally from residue Y22, there were significant contributions from the other residues too. In order to get atomistic insights into the origins of these contributions, crystallography correlated with Isothermal Calorimetry (ITC) would be required. While the authors did not embark on structural characterization of all 12 mutants, they did crystallize one and this provided some insights into structure–activity relationships. We have demonstrated that dynamics plays a crucial role in modulating the interactions between p53 and MDM2 [14–16] using the techniques of molecular simulations, which have also been successfully used in several other systems [17]. While the reproduction of absolute free energies from simulations is still not achievable [18], nevertheless the relative affinities and the underlying trends are increasingly being captured by simulation methods [17, 19]. For the current study, the experimental data provide a very good test set to benchmark simulation methods that employ molecular dynamics (MD) simulations. If a proper benchmark is established, then the protocol may be used to design tight-binding peptides. In the current study, we enquire whether it is possible to estimate the trends in experimental binding affinities by running several short simulations, or does one need long simulations. The current work is carried out in the spirit of a study [20], which demonstrated that the conformational space that is covered over ten short simulations is greater than that covered by one long simulation.

2 Methods

The crystal structure of MDM2 complexed with the peptide PMI (crystal structure 3EQS, resolution 1.65 Å [11]) was used for this study. Each amino acid of PMI was mutated to alanine (except residue 4 which already is an alanine) separately leading to 11 systems. Residues 25–109 of MDM2 were included in these studies for which the missing residue E25 was modelled using PyMOL [21]; similarly, we also modelled P12 of PMI as it was missing in the crystal structure. For each mutant sequence derived from PMI, 10 models were generated using MODELLER 9v8 [22] with the crystal structure of 3EQS as the template. MODELLER works by satisfying spatial restraints that are derived from an alignment of the sequence of the protein whose three-dimensional structure has to be constructed (the complex of the PMI peptides with MDM2) with the sequence of the protein whose three-dimensional structure is available from experiments such as crystallography (3EQS in this study). The program optimizes a molecular probability density function with the variable target

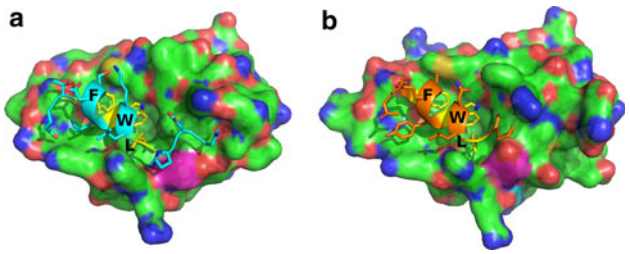

Fig. 1 The structure of the p53 peptide in cyan ribbon and sticks (the carbon, nitrogen and oxygen atoms are coloured *cyan*, *blue* and *red,* respectively) complexed to the N-terminal domain of MDM2 (coloured surface where the carbon, nitrogen and oxygen atoms are coloured *green*, *blue* and *red,* respectively) taken from the crystal structure 1YCR (Kussie et al.) on the *left* (**a**) and the structure of the PMI peptide in orange ribbon/sticks (the carbon, nitrogen and oxygen atoms are coloured *orange*, *blue* and *red,* respectively) complexed to the N-terminal domain of MDM2 (*coloured surface* where the carbon, nitrogen and oxygen atoms are coloured *green*, *blue* and *red,* respectively) taken from the crystal structure 3EQS (Pazgier et al. 2009) on the *right* (**b**). The three key hydrophobic residues that embed into the surface of MDM2, i.e. F19, W23 and L26 are shown as *yellow* sticks (the carbon and nitrogen atoms are coloured *yellow* and *blue,* respectively); only the Cα atoms from the backbone and the non-hydrogen atoms of the sidechains are shown for clarity

function procedure in Cartesian space, which uses conjugate gradient algorithms and molecular dynamics with simulated annealing. Each model was solvated using the TIP3P water model with a 12 Å minimum distance between solute and box boundary and neutralized using Cl^- ions as appropriate (for the wild-type system, we added 4 Cl^- ions, while for the alanine scan, we added either 4 or 5 Cl^- ions depending on the residue being changed) using the TLEAP module of AMBER11 [23, 24]. The total number of atoms including water molecules ranged from 19,257 to 24,119 across the various systems. MD simulations were performed using the PMEMD module, where each of the ten models was first minimized for 4000 steps using the ff99SB force field [25]. Subsequently, employing a 2-fs time step, and SHAKE [26] on the hydrogen atoms, each model was heated to 300 K over 30 ps, equilibrated for 100 ps, simulated for a production run of 100 ps. Excluding heating, this resulted in a total of 1 ns for each peptide sequence. Binding enthalpies were calculated using the MMGBSA script of AMBER11 over 500 frames (50 snapshots taken every 2 ps for each of the 10 models), while entropic contributions were estimated using normal mode analysis from 50 frames (five snapshots taken every 10 ps, multiplied by 10 models). To compare the averages over the ten short simulations of 100 ps duration each, we carried out one long simulation (50 ns) of the wild-type peptide, of which the last 40 ns were analysed. Binding enthalpies were calculated over 5,000 frames spaced 8 ps apart, while normal mode analysis was carried out over 50 frames, spaced 800 ps apart.

While the crystal structures depict the PMI peptides as being helical when complexed with MDM2, we have previously shown for p53 that the bound conformation of the peptides can vary significantly and yet yield very similar values of binding free energies [15]. Bearing this in mind, we extended the current study for the 11 peptides complexed to MDM2, where the conformations of the peptides at their C-termini were changed to an extended state. This was modelled based on the conformation of p53 in its complex with MDM2 as seen in the crystal structure 1YCR (resolution 2.6 Å, [27]) and as shown in Fig. 1a.

The numbering scheme used in our study refers to the p53 sequence as numbered from 17 to 29 (ETFSDLW KLLPEN) and the PMI sequence as numbered from 1 to 12 (TSFAEYWNLLSP). In these studies, we use ΔG to refer to absolute values that have been either computed or experimentally determined and ΔΔG mainly for comparing the ala scan with other methods.

3 Results

We generated ten models for each mutation using MODELLER and used them as starting points for the MD simulations in this study to ensure diversity in the sampling of the phase space for each peptide–MDM2 complex. The models generated by MODELLER varied by ∼0.1 Å over all Cα atoms and ∼0.2 Å over all non-hydrogen atoms (Fig. 2), although positional differences in sidechain atoms can be as large as 6 Å. The residues that are buried are very similar to each other in conformations while the exposed residues vary significantly. This ensures that the MD simulations cover a wider range of phase space than would be covered by a single starting structure. A comparison of the energies of binding of PMI to MDM2 (Table 1) shows that the average over ten short simulations of duration 100 ps each yields values of enthalpies of binding that are very similar to those obtained from averaging over 40 ns. The use of the shorter simulations resulted in savings of computational times of the order of 25-fold. The dominant contribution to overall binding is van der Waals (Table 2) and is in agreement with what we and others have demonstrated earlier [12, 16, 28, 29], arising from the three critical amino acids, F19, W23 and L26. There is some difference in the electrostatic contributions, although they are within the standard deviation; in any case, the electrostatic interactions are offset by desolvation penalties. We next asked what the energies would be if we had run the simulations for 10, 20 or 30 ns only. The data in Table 2 suggest that they all yield values that are similar to the 40 ns analysis, and all the components are within 5% of each other, suggesting that perhaps the use of shorter simulations may be beneficial in terms of the savings in

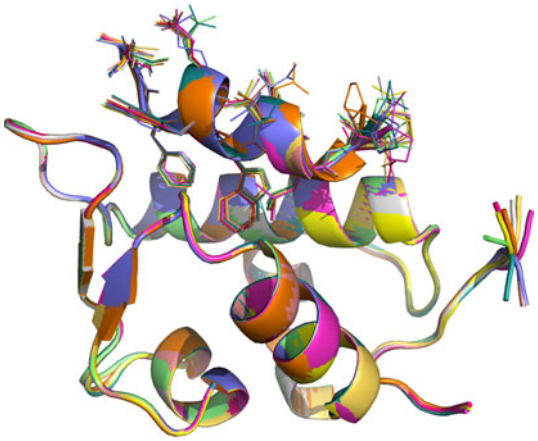

Fig. 2 The ten conformations generated using MODELLER show the variations in the structures of the models that are used as starting points for each mutant peptide in our study. This figure shows the structures of ten models of wild-type PMI complexed to MDM2. The sidechains of the peptide are shown to highlight the variations in their rotamers. It is clear that the buried sidechains do not vary much in conformations, while the exposed residues can vary significantly. For clarity, only the peptide sidechains are shown

Table 1 The computed enthalpies, entropies and free energies of the binding of wild-type PMI to MDM2 from a long (50 ns) and 10 short (100 ps) simulations (peptide is helical in the complex)

	ΔH (kcal/mol)	$T\Delta S$ (kcal/mol)	ΔG (kcal/mol)
Last 40 ns of 50 ns	−48.3 ± 3.9	−34.11 ± 3.9	−14.2
10 * (last 100 ps of 200 ps)	−49.6 ± 4.0	−32.7 ± 3.7	−16.8

computational times and at the same time, yield trends that are in agreement with the trends seen in the experimentally determined free energies.

Having established the benchmark, we next proceeded to compute the enthalpies, entropies and free energies for the alanine-scanned peptides over the ten short simulations for each peptide and over several windows of time. The results are shown graphically in Fig. 3. The correlations between the estimated free energies across the various time windows and the experimental affinities range from 0.65 to 0.71, with greater significance apparent only for the enthalpic changes. Indeed the enthalpies correlate between 0.79 and 0.92, which are quite good; the entropies, unsurprisingly, do not appear to be well represented [30]. This is not surprising given that the computations of entropy still suffer from significant approximations [17]. Moreover, while there will be an a non-negligible entropic contribution, for example, arising from displacement of water molecules, nevertheless the entropic contributions to the overall free energy changes for the various peptides are likely to be similar. What is interesting in our study is that the correlations only increase by 7% when the simulation times are increased by tenfold, from 100 ps to 1 ns. The promising observations are that the hydrophobic tetrad of W7, F3, L10 and Y6 appears to be the most perturbed by the alanine mutations, as has been observed experimentally [13]. Indeed, the only component of the enthalpy that is significantly correlated to the experimental affinities is the van der Waals interaction energy, thus underscoring the dominance of packing in the interactions of these peptides with MDM2. The tetrad residues F3, Y6, W7 and L10 undergo losses in van der Waals interaction energies of approximately 9, 9, 13 and 6 *kT,* respectively. When T1 is mutated to an alanine, the loss of experimental affinity has been attributed to the destabilization of the helicity of the peptide owing to disruption of helix capping; our simulations show that in addition, the methyl group of the sidechain of Thr packs against the phenolic sidechain of Y6 which in turn derives free energy by packing against H73 (Fig. 4a). Upon mutation of T1A, the packing of this methyl is lost and the Y6 group disengages from the packing, leading to a destabilization of the van der Waals interaction energies by $\sim$5 *kT*. In the S2A mutation, the loss of stabilization of the helix is partly compensated by the formation of stronger hydrogen bonds between the sidechain of Q72 and the backbone amide of F3, which is now exposed; this incurs an electrostatic gain of $\sim$2 *kT* inclusive of desolvation penalty. The F3A mutation as expected incurs a large loss of van der Waals interaction energy (8 *kT*), and the associated local perturbations lead to a 12 *kT* loss of electrostatic stabilization, which is reduced by the solvation of exposed polar groups. The E5A mutation was experimentally shown to cause moderate reduction in binding affinity, originating in the loss of hydrogen bonds that stabilize the helix. In addition, the current

Table 2 The computed binding enthalpies (in kcal/mol) and components (in kcal/mol) across different time windows for the binding of wild-type PMI to MDM2

	PMI (100 fs)	PMI 40 ns	PMI 30 ns	PMI 20 ns	PMI 10 ns
ΔH (kcal/mol)	−49.6 ± 4.0	−48.3 ± 3.9	−48.2 ± 4.1	−47.9 ± 4.2	−47.3 ± 3.9
ELEC (kcal/mol)	−174.9 ± 35.2	−161.4 ± 27.5	−166.5 ± 28.7	−164.9 ± 28.5	−159.2 ± 21.6
VDW (kcal/mol)	−65.5 ± 4.3	−64.2 ± 4.3	−64.7 ± 4.4	−65.7 ± 4.3	−65.7 ± 4.7
GB (kcal/mol)	200.0 ± 33.3	185.9 ± 26.4	191.7 ± 26.9	191.5 ± 26.5	186.4 ± 21.2
GBSOL (kcal/mol)	190.8 ± 33.3	177.3 ± 26.3	182.9 ± 26.9	182.7 ± 26.5	177.6 ± 21.1

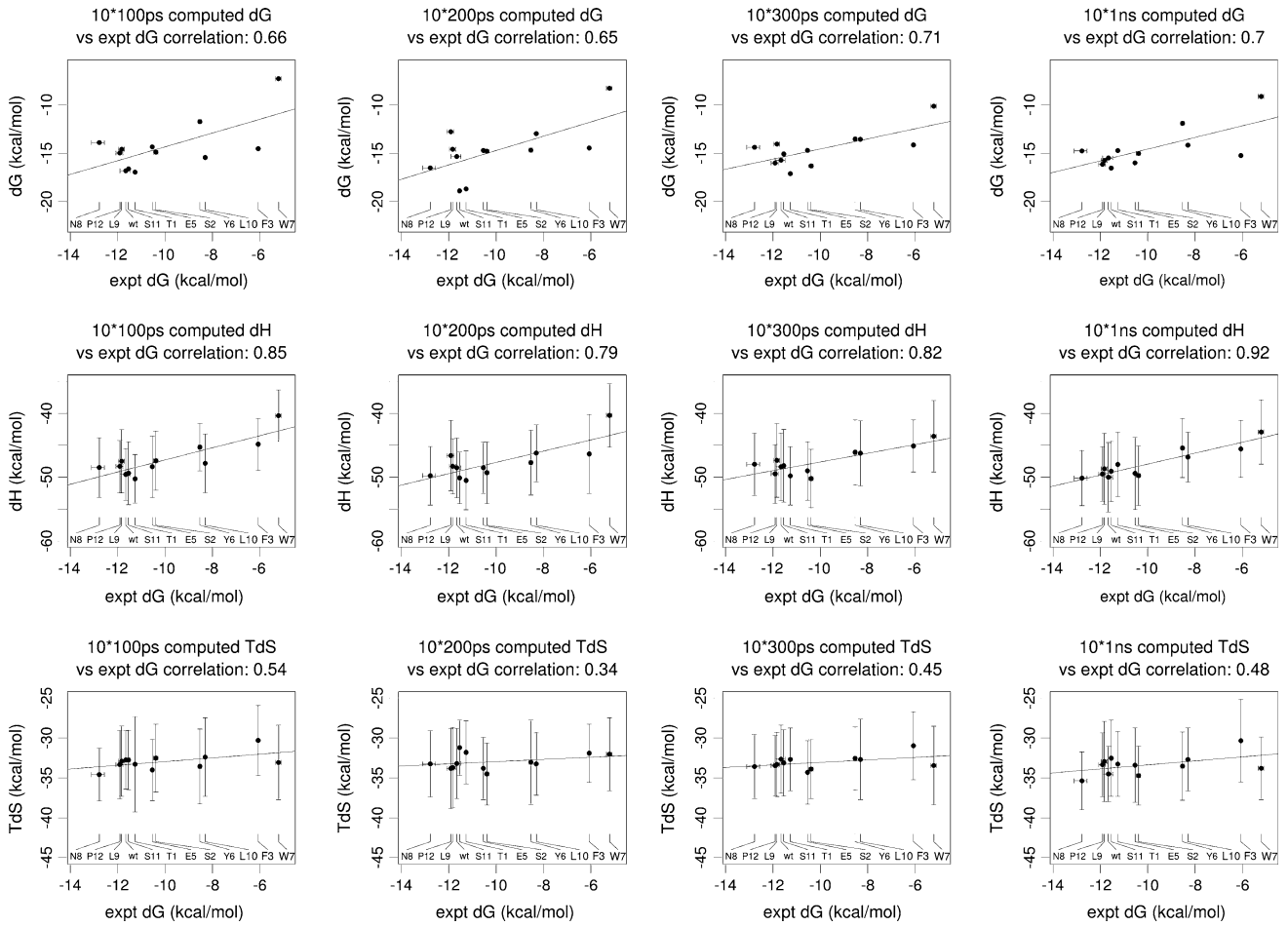

Fig. 3 The correlations of the computed free energy, enthalpy and entropies using the MMGBSA protocol with normal-mode-based entropies for the binding of the ala scan mutants of PMI to MDM2 with the experimentally determined free energies of binding for simulations times of 100 ps, 200 ps, 300 ps and 1 ns. The standard deviations across the simulations, including block averages, are ~10% of the mean values reported in the table, thus yielding an error of ~1–2 kcal/mol

simulations reveal that the Glu sidechain formed dynamic hydrogen bonds with the sidechain and backbone amide of S2, thereby partly "locking the sidechain of T1 in a position where it packed against Y6. The loss of the E6 sidechain relieves this lock somewhat, and the loss of the packing of the T1 against Y6 leads to a destabilization of the van der Waals interactions by ~1.5 *kT* (Fig. 4b). The loss of the sidechain of Y in Y6A causes significant loss of packing, and the associated van der Waals penalty is ~9 *kT*. At the same time, Y6 forms transient hydrogen bonds (lifetimes of 20 ps) with the sidechain of K94 which are now lost, leading to an electrostatic penalty of ~11 *kT* which is compensated for by the relief of desolvation costs. The mutation W7A causes the maximal loss of van der Waals (~12 *kT*) amongst all the mutants; this is experimentally the most destabilized mutant. In addition, there is the loss of the indole-Leu54 carbonyl hydrogen bond that destabilizes the electrostatics by ~5 *kT*. The N8A mutation in our simulation studies improves the overall binding by a small amount; experimentally, it lead to a very high-affinity peptide. While the crystal structures did not really reveal any major differences from the wild type, the authors concluded that small subtle changes that appear to stabilize the helix and tend to accumulate, lead to the high affinity. In the simulations, it is evident that N8 is largely solvent exposed but does transient hydrogen bond (lifetimes of up to 80 ps) to the sidechain of S11 and the backbone carbonyl of A4. The loss of hydrogen bonds leads to destabilized electrostatics, which are compensated for by the solvation effects of the exposed polar atoms. A comparison of the crystal structure of the N8A mutation (3LNZ, resolution 1.95 Å [13]) and the modelled structure shows that the simulations reproduce the experimental data remarkably well (Fig. 4c). The mutation L9A does not cause significant changes since L9 is largely solvent exposed; its mutation to alanine only results in some local packing destabilization (~3 *kT*). L10 is packed between the peptide and MDM2 and its mutation to alanine leads to

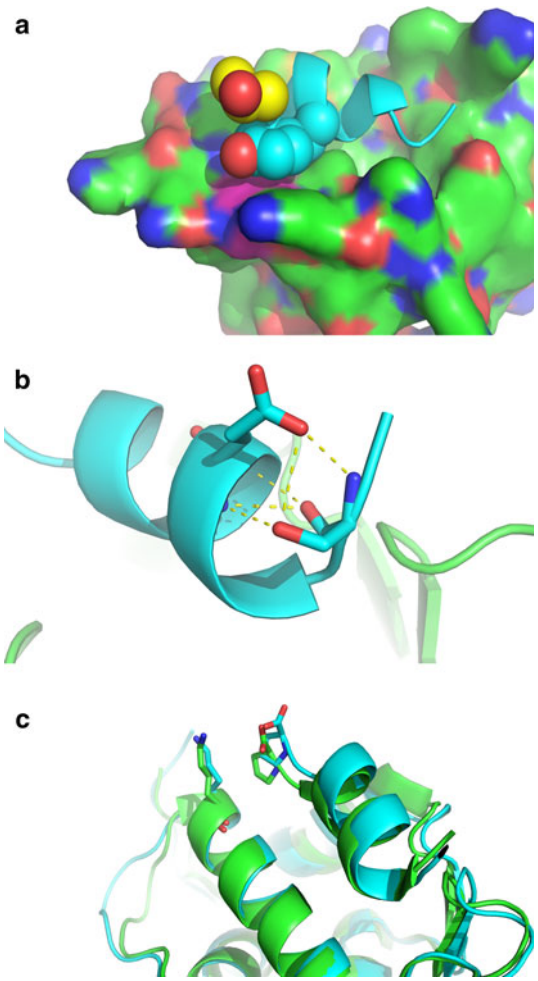

Fig. 4 **a** The stacking of Y6 between T1 and His73-MDM2 taken from the crystal structure 3EQS.pdb of the PMI peptide (cartoon with Y6 sidechain in *spheres*; carbon, and oxygen atoms are shown in *cyan*, and *red,* respectively; T1 sidechain is shown as *spheres* with carbon, oxygen in *yellow* and *red* colours, respectively) complexed with MDM2 (carbon, nitrogen and oxygen atoms in *green*, *blue* and *red,* respectively; the His73 is coloured with carbon, nitrogen and oxygen in *magenta*, *blue* and *red,* respectively). **b** S3 and E5 of PMI interact through hydrogen bonds (*dashed yellow lines*) to stabilize the helix of PMI (*cyan*) against the MDM2 (*green*). **c** The N8A mutant version of PMI complexed to MDM2 taken from the crystal structure 3LNZ (in *green*) and the final snapshot of one of the simulations from the 10 1-ns simulations (in *cyan*). The C-terminal Pro of the peptide and Lys51 of MDM2 are shown in sidechains

a packing loss of $\sim 6\ kT$. The S11A mutation results in local packing destabilization ($\sim 3\ kT$), and the associated loss of the hydrogen bond to N8 sidechain incurs electrostatic penalties that are compensated for by solvation effects. The P12A mutation relieves the constraint on the carboxy terminus, which now forms long-lived hydrogen bonds with the sidechain of Ly51. While the loss of the P12 packing incurs a van der Waals penalty of $\sim 3.5\ kT$, the electrostatics are stabilized significantly; of course, they are offset by the desolvation penalties, resulting in a net gain of only $\sim 3\ kT$. These 1-ns simulations appear to be a good compromise between a fairly good correlation between the computed and experimental data and also appear to provide mechanisms behind the observed changes in affinities.

4 Discussion

The field of peptide design has made tremendous progress in recent years stemming from the development of several methods for designing/optimizing peptides/peptidomimetics for specific functions including, increasingly, for therapy [31]. One of the major advances stems from the ideas developed by James Wells [32] that aim to identify hot spots through alanine-scanning mutagenesis. These yield regions of a peptide/protein that are candidates for mutagenesis to improve or destabilize interactions. This received a great boost when Massova and Kollmann [33] introduced a simple protocol of computational alanine scanning. In effect, these attempts to identify the hot spots by carrying out an MD simulation on a protein–peptide complex and then each snapshot is manipulated by mutating a specific residue to alanine and computing the energetic changes relative to the wild type. The philosophy was given a further boost through the availability of web-based protocols for rapid identifications of hot spots by the group of David Baker [34, 35]. Several other studies have taken this protocol forward with individual tweeks to the basic philosophy with varying results, including the original work of Kollman which examined the MDM2-p53 interface [33], a TCR-p-MHC complex [36] (with a correlation of around 0.7 with respect to the experimental affinities, similar to that found by Massova and Kollman), trypsin–peptide interactions [17] (correlations between computed and experimental affinities of ~ 0.9). In a very detailed look at several protocols, including running 10-ns simulations on each alanine mutation, Bradshaw et al. [17] used a trypsin-peptide system and showed that the methodology of Kollman gives the best performance. Indeed their computations yielded the correct ranking of the mutational effects. They do caution that such methods may yet be found to be sensitive to system details and highlighted a caveat that MD simulations on mutants may enable the sampling of conformational changes, which will not be captured by the Kollman method. Our method is a variant on the Kollman theme and is performed to investigate whether short bursts of simulations can capture the conformational properties of these mutations [20] and yet remain computationally inexpensive. We apply this method using a dataset generated from the experiments of Li et al. [13], where the authors characterize the contributions of each residue of a 12 residue peptide that binds the protein

MDM2 with a high affinity. We find that the correlations between the computed values with respect to the experimental binding affinities are quite respectable when only the enthalpic terms are taken into account. Although they appear to improve somewhat with the simulation times, the improvement is a mere 7%, in contrast to the tenfold increase in simulation time. While our method needs investigations to improve the entropic estimates, it does reproduce the experimental observation that the hydrophobic tetrad is the most highly destabilized upon mutation; in addition, the 1-ns simulations show that the mutation that enhances the affinity most in the experiments, N8A, is also found to be the most stable in our study. One of the limitations of our study is that there are several water molecules that mediate interactions between the peptide and MDM2 (Fig. 5). While they have been accounted for in the simulations, we have not included them for our energetic analysis. That such waters indeed would have contributed to the energetics has been outlined in some studies [36]; recent work has been highlighting the intimate role of water molecules in recognition and binding of proteins and peptides [37, 38]. How does our protocol compare with the Kollman protocol as included in the AMBER software and with the Baker protocol as defined in the Robetta web server (http://www.robetta.bakerlab.org/alascansubmit.jsp)? The AMBER protocol was used to compute the affinities over the last 40 ns of the 50 ns. Both protocols produce excellent overall correlations of around 0.9 (Fig. 6a). Both protocols do very well at reproducing the overall correlation; however, these appear to be skewed as are our own results, stemming from a very good correlation arising from the reproduction of the trends of the hydrophobic tetrad properties. Disappointingly, the trends for the rest of the residues are not very good across all the methods; indeed our method appears to do a little better than the others (Fig. 6b). The one feature that remains in favour of our method is that the computations are carried out in explicit solvent followed by estimation of binding energies in a generalized born model. The Robetta method describes the affinities in terms of empirically derived potentials, while in the AMBER protocol, only the wild-type dynamics are computed in explicit water while the affinities of the mutants are estimated in a continuum approximation for bulk solvent. We are currently exploring such comparative studies to systems without such dominant hydrophobic interactions driving the binding. In addition, the fact that entropies are not computed so well is another limitation; careful manipulation of entropic effects can be useful for the design of novel peptides with higher affinities [39]. Finally, we also note in the 50-ns simulations (data to be presented elsewhere) that the C-terminus of the peptide does undergo conformational switching between the crystallographically observed helical conformation and the more extended conformation seen in the crystal structure of p53 complexed with MDM2 in 1YCR [27] and the one modelled in an earlier work [15]. Therefore the alanine scan was carried out for the PMI peptide, which was modelled with an extended C-terminus (Table 3; Fig. 6a, b). While the overall correlations do not change much, it is promising that there is an improvement in the non-tetrad region. Curiously, the experimental trends followed by the most stabilizing (relative to wild-type) mutants, i.e. N8A followed by L9A are best reproduced by the C-terminal extended simulations. This may perhaps originate in the ability of the C-terminus to toggle between the helical and extended states; our earlier work [15] had demonstrated that while the P27S mutant of the p53 peptide exists in a conformation that is extended at the C-terminus as observed in the crystal structure 1YCR, it can also exist in a helical conformation and both conformations appeared to contribute equivalent amounts of binding energy. Thus, our current finding further strengthens that hypothesis and suggests that computations of binding affinities may need to carefully account for conformations other than those derived from crystal structures, at least in some systems. Indeed, it is unlikely that this protocol will succeed with every topology. It is likely that the reason why this works well in systems such as the PMI–MDM2 interactions is because PMI assumes a helical fold that is nicely sequestered in the MDM2-binding pocket; indeed even if the C-terminal region is extended, nevertheless the overall helical fold is quite robust when bound. These peptides bind through several anchor points—in this case through F3, W7 and L10. This implies that large perturbations such as F > A or W- > A are easily compensated for by the rest of the robust helical fold, and hence the binding energetics are easily captured by the short simulations. In fact, deviations are evident in the fact that when the non-tetrad

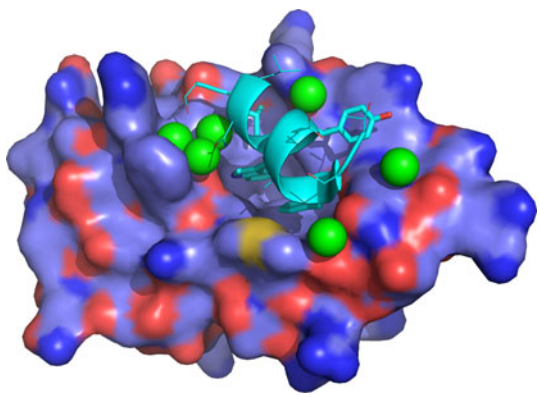

Fig. 5 PMI (*cyan*) complexed to MDM2 (surface) taken from the crystal structure 3EQS.pdb, showing the water molecules (*green spheres*) that mediate hydrogen bonds between the peptide and MDM2

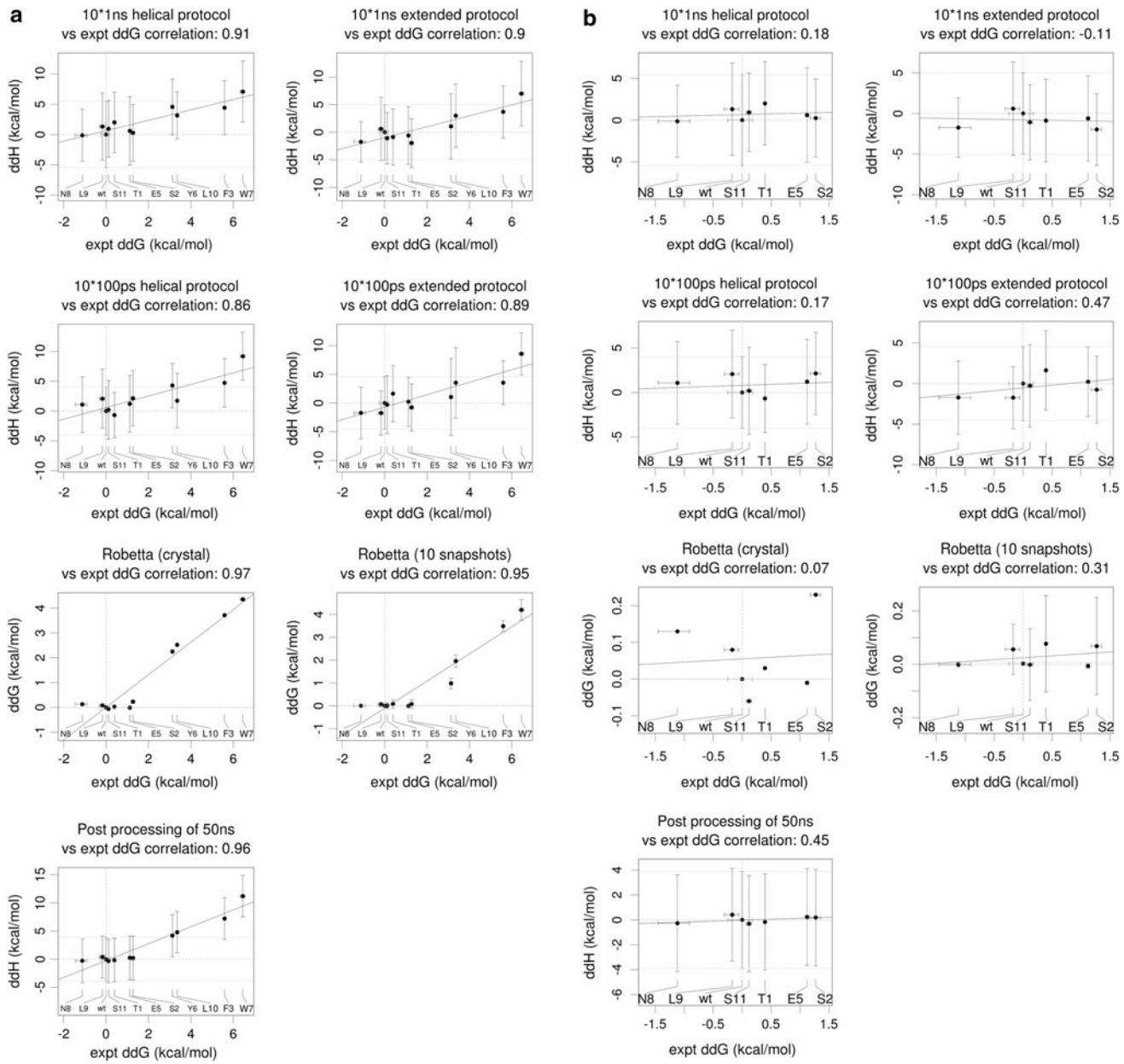

Fig. 6 **a** Correlations of the binding enthalpies computed using different protocols against the experimental affinities. **b** Correlations of the binding enthalpies of the non-hydrophobic tetrad residues computed using different protocols against the experimental affinities; helical and extended protocols refer to the peptides in helical conformations (as seen in the crystal structure 3EQS of the PMI peptide complexed to MDM2) or in conformations with the C-terminal modelled in extended conformations as in the crystal structure 1YCR of the p53 peptide complexed to MDM2. Postprocessing of 50 ns refers to the ala scan carried out based on the AMBER protocol. Robetta server (robetta.bakerlab.org) was used for ala scan for the crystal structure and for ten snapshots taken from the 1-ns MD simulation. The standard deviations across the simulations, including block averages, are $\sim$10% of the mean values reported in the table, thus yielding an error of $\sim$1–2 kcal/mol

regions are examined, the correlation between computed and experimental data becomes poor. In the current study, the standard deviations are of the order of 10 kcal/mol (errors of the order of 1–2 kcal/mol) and this leads to various overlaps in the plots, thus reducing the net correlations. This magnitude corresponds to a hydrogen bond and can have significant effects on the binding affinity and often can mean the difference between a good binder and an extremely good binder [40]. It will be interesting to examine the robustness of the computations if small to large mutations are carried out. Nevertheless, the current findings do offer promise in speeding the design of peptides with enhanced affinities, albeit for a small class of systems.

Table 3 The relative changes in computed/experimental affinities (in kcal/mol) with respect to the wild-type PMI for the various protocols (Robetta alanine scan from http://www.robetta.bakerlab.org/alascansubmit.jsp)

Position	Experimental	10 × 1 ns helical	10 × 100 ps helical	10 × 100 ps extended	Robetta crystal structure (10 Snapshots average)	AMBER alanine scan (postprocessing)
T1	0.39	2.00	−0.68	1.63	0.03 (0.08)	−0.17
S2	1.27	0.25	2.14	−0.76	0.23 (0.07)	0.19
F3	5.59	4.42	4.73	3.55	3.71 (3.49)	7.21
A4	0.00	0.00	0.00	0.00	0.00 (0.00)	0.00
E5	1.12	0.60	1.21	0.21	−0.01 (−0.01)	0.23
Y6	3.13	4.56	4.27	1.05	2.25 (0.98)	4.17
W7	6.45	7.07	9.20	8.58	4.35 (4.20)	11.19
N8	−1.12	−0.13	1.08	−1.72	0.13 (0.00)	−0.27
L9	−0.17	1.31	2.07	−1.74	0.08 (0.06)	0.41
L10	3.35	3.14	1.73	3.54	2.52 (1.96)	4.78
S11	0.12	0.93	0.19	−0.27	−0.06 (0.00)	−0.31
P12	−0.25	0.50	1.26	−0.93		

The computed affinities are the enthalpic components only

5 Conclusions

In conclusion, our study suggests that computational alanine scans of peptide–protein interfaces can yield promising hot spots for mutagenesis studies by running multiple short simulations in explicit water of each alanine mutation and brings about significant reductions in computational costs. We further find that in some systems, such as the p53-peptides, accounting for the conformational variability of the peptides explicitly leads to improvements in the computed properties. Conformations not seen crystallographically, yet guided by spectroscopies such as CD, must be modelled and their effects included in the analyses; these give insights into the nature and diversity of the complex dynamics that characterize the interactions and may not be immediately obvious from the crystal structures alone; indeed it was the incorporation of these that appeared to improve the computed affinities for some of the mutants. However, modelling the entropic contributions still needs improvements and further work is needed to examine the effects of small to large mutations.

References

1. Brown CJ, Lain S, Verma CS, Fersht AR, Lane DP (2009) Awakening guardian angels: drugging the p53 pathway. Nat Rev Cancer 9:862–873
2. Wade M, Wang YV, Wahl GM (2010) The p53 orchestra: Mdm2 and Mdmx set the tone. Trends Cell Biol 20:299–309
3. Meek DW, Anderson CW (2009) Posttranslational modification of p53: cooperative integrators of function. Cold Spring Harb Perspect Biol 1:a00950
4. Wallace M, Worrall E, Pettersson S, Hupp TR, Ball KL (2006) Dual-site regulation of MDM2 E3-ubiquitin ligase activity. Mol cell 23:251–263
5. Schon O, Friedler A, Bycroft M, Freund SMV, Fersht AR (2002) Molecular mechanism of the interaction between MDM2 and p53. J Mol Biol 323:491–501
6. Bottger A, Bottger V, Garcia-Echeverria C, Chene P, Hochkeppel HK, Sampson W, Ang K, Howard SF, Picksley SM, Lane DP (1997) Molecular characterization of the hdm2–p53 interaction. J Mol Biol 269:744–756
7. Brown CJ, Cheok CF, Verma CS, Lane DP (2011) Reactivation of p53: from peptides to small molecules. Trends Pharmacol Sci 32:53–62
8. Reifenberger G, Liu L, Ichimura K, Schmidt EE, Collins VP (1993) Amplification and overexpression of the MDM2 gene in a subset of human malignant gliomas without p53 mutations. Cancer Res 53:2736–2739
9. Onel K, Cordon-Cardo C (2004) MDM2 and prognosis. Mol Cancer Res 2:1–8
10. Cheok CF, Verma CS, Baselga J, Lane DP (2011) Translating p53 into the clinic. Nat Rev Clin Oncol 8:25–37
11. Pazgier M, Liu M, Zou G, Yuan W, Li C, Li C, Li J, Monbo J, Zella D, Tarasov SG, Lu W (2009) Structural basis for high-affinity peptide inhibition of p53 interactions with MDM2 and MDMX. Proc Natl Acad Sci USA 106:4665–4670
12. Joseph TL, Madhumalar A, Brown CJ, Lane DP, Verma CS (2010) Differential binding of p53 and nutlin to MDM2 and MDMX: computational studies. Cell Cycle 9:1167–1181
13. Li C, Pazgier M, Li C, Yuan W, Liu M, Wei G, Lu WY, Lu W (2010) Systematic mutational analysis of peptide inhibition of the p53-MDM2/MDMX interactions. J Mol Biol 398:200–213
14. Chen HF, Luo R (2007) Binding induced folding in p53-MDM2 complex. J Am Chem Soc 129:2930–2937
15. Dastidar SG, Lane DP, Verma CS (2009) Multiple peptide conformations give rise to similar binding affinities: molecular simulations of p53-MDM2. J Am Chem Soc 130:13514–13515
16. Dastidar SG, Madhumalar A, Fuentes G, Lane DP, Verma CS (2010) Forces mediating protein–protein interactions: a computational study of p53 "approaching" MDM2. Theoret Chem Acc 125:621–635

17. Bradshaw RT, Patel BH, Tate EW, Leatherbarrow RJ, Gould IR (2011) Comparing experimental and computational alanine scanning techniques for probing a prototypical protein–protein interaction. Prot Eng Des Sel 24:197–207
18. Deng Y, Roux B (2009) Computations of standard binding free energies with molecular dynamics simulations. J Phys Chem B 113:2234–2246
19. Knight JL, Brooks CL III (2011) Surveying implicit solvent models for estimating small molecule absolute hydration free energies. J Comput Chem 32:2909–2923
20. Caves LS, Evanseck JD, Karplus M (1998) Locally accessible conformations of proteins: multiple molecular dynamics simulations of crambin. Protein Sci 7:649–666
21. The PyMOL Molecular Graphics System, Version 1.2r1, Schrödinger, LLC
22. Sali A, Blundell TL (1993) Comparative protein modelling by satisfaction of spatial restraints. J Mol Biol 234:779–815
23. Case DA, Cheatham TE III, Darden T, Gohlke H, Luo R, Merz KM Jr, Onufriev A, Simmerling C, Wang B, Woods RJ et al (2005) The Amber biomolecular simulation programs. J Comput Chem 26:1668–1688
24. Ponder JW, Case DA (2003) Force fields for protein simulations. Adv Protein Chem 66:27–85
25. Hornak V, Abel R, Okur A, Strockbine B, Roitberg A, Simmerling C (2006) Comparison of multiple Amber force fields and development of improved protein backbone parameters. Proteins 65:712–725
26. Ryckaert JP, Ciccotti G, Berendsen HJC (1977) Numerical integration of the cartesian equations of motion of a system with constraints: molecular dynamics of n-alkanes. J Comput Phys 23:327–341
27. Kussie PH, Gorina S, Marechal V, Elenbaas B, Moreau J, Levine AJ, Pavletich NP (1996) Structure of the MDM2 oncoprotein bound to the p53 tumor suppressor transactivation domain. Science 274:948–953
28. Zhong H, Carlson HA (2005) Computational studies and peptidomimetic design for the human p53-MDM2 complex. Proteins 58:222–234
29. Carotti A, Macchiarulo A, Giacche N, Pellicciari R (2009) Targeting the conformational transitions of MDM2 and MDMX: insights into key residues affecting p53 recognition. Proteins 77:524–535
30. Yang T, Wu JC, Yan C, Wang Y, Luo R, Gonzales MB, Dalby KN, Ren P (2011) Virtual screening using molecular simulations. Proteins 79:1940–1951
31. Mason JM (2010) Design and development of peptides and peptide mimetics as antagonists for therapeutic intervention. Future Med Chem 2:1813–1822
32. Wells JA (1991) Systematic mutational analysis of protein–protein interfaces. Methods Enzymol 202:390–411
33. Massova I, Kollman PA (1999) Computational alanine scanning to probe protein–protein interactions: a novel approach to evaluate binding free energies. J Am Chem Soc 121:8133–8143
34. Kortemme T, Kim DE, Baker D (2004) Computational alanine scanning of protein–protein interfaces. Sci STKE 219:l2
35. Kortemme T, Baker D (2002) A simple physical model for binding energy hot spots in protein–protein complexes. Proc Natl Acad Sci USA 99:14116–14121
36. Zoete V, Michielin O (2007) Comparison between computational alanine scanning and per-residue binding free energy decomposition for protein–protein association using MM-GBSA: application to the TCR-p-MHC complex. Proteins 67:1026–1047
37. Ahmad M, Gu W, Geyer T, Helms V (2011) Adhesive water networks facilitate binding of protein interfaces. Nat Commun 2:261
38. Thirumalai D, Reddy G, Straub JE (2011) Role of water in protein aggregation and amyloid polymorphism. Acc Chem Res (in press) doi:10.1021/ar20000869
39. Madhumalar A, Lee HJ, Brown CJ, Lane DP, Verma CS (2009) Design of a novel MDM2 binding peptide based on the p53 family. Cell Cycle 8:2828–2836
40. Zondlo SC, Lee AE, Zondlo NJ (2006) Determinants of specificity of MDM2 for the activation domains of p53 and p65: proline 27 disrupts the MDM2-binding motif of p53. Biochemistry 45:11945–11957